ELSEVIER

Surface Science 431 (1999) 96–108

surface science

www.elsevier.nl/locate/susc

# Direct STM observation of surface modification and growth of AgCl islands on Ag(111) upon chlorination at room temperature

B.V. Andryushechkin, K.N. Eltsov*, V.M. Shevlyuga, V.Yu. Yurov

*Natural Science Center, General Physics Institute RAS, Vavilov str. 38, 117942 Moscow, Russia*

Received 22 August 1998; accepted for publication 13 March 1999

**Abstract**

The results of STM, AES and TDS study of a Ag(111) surface treated by molecular chlorine in UHV with doses up to 100 000 L are presented. We obtained direct evidence of AgCl island formation on the surface upon chlorine adsorption at room temperature. The specific feature of the modified silver surface is AgCl islands surrounded by ditches with 50–150 Å depth and untreated atomic plateaux. The atomic structure and chemical state of the surface area with no AgCl islands corresponds to saturated chlorine monolayer with a Ag(111)-$(17\times17)$-Cl structure. A strong influence of AES primary electron beam on the morphology of the silver chloride film was observed by STM. A small (0.1 C $cm^{-2}$) electron beam dose caused a tremendous modification of the AgCl island film forming 'giant' AgCl islands surrounded by a smooth surface covered by chemisorbed chlorine. This surface modification could be an origin of discrepancy in the interpretation of previous electron spectroscopy results. © 1999 Elsevier Science B.V. All rights reserved.

*Keywords:* Atomic structure; Chloride islands; Chlorination; Electron beam action; Scanning tunnelling microscopy (STM); Ultra-high vacuum

## 1. Introduction

The interaction of molecular chlorine with silver crystals is of considerable interest because of an important role of chlorine-containing molecules in the ethylene epoxidation process [1–3]. A small amount of such molecules in a reactor strongly improves (up to 85% [3]) the selectivity of the reaction. Since the classical papers of Rovida et al. [4], Goddard and Lambert [5], and Tu and Blakely [6] on chlorination of low-index planes of silver in ultra-high vacuum, almost all investigations have been made from this point of view. According to common opinion, chemisorbed chlorine acts as a promoter, and silver chloride as a poison, in ethylene epoxidation [1–3,7]. Therefore, all these studies aimed to characterize the chlorine chemisorption and silver chloride formation processes. Unfortunately, there is no direct evidence of this confirmation up to now; moreover, it is not so easy to create the conditions of chloride formation on a clean silver surface. It was shown in Ref. [8] that a first step of direct deposition of silver chloride on silver was the formation of a chemisorbed chlorine monolayer. The growth of a silver chloride film was possible only after filling of the monolayer coverage. In this sense, the role of

* Corresponding author. Fax: +7-095-1326001.
*E-mail address:* eltsov@kapella.gpi.ru (K.N. Eltsov)

0039-6028/99/$ – see front matter © 1999 Elsevier Science B.V. All rights reserved.
PII: S0039-6028(99)00429-X

chlorine in ethylene epoxidation by a silver catalyst remains unclear.

Another interesting problem stimulating the study of silver chlorination in UHV is the possible application of small photosensitive silver chloride particles on a metal surface for nanotechnology based on controllable reduction of chloride by electron or light beams[1]. Such chloride nanoobjects could be formed by chlorine adsorption or silver chloride deposition.

Attention to the mechanism of silver chlorination has been focused in 80-s [9–13]. In spite of the considerable age of these investigations, many questions still remain open. One of the unclear points is the mechanism of nucleation and growth of chloride phase. Electron spectroscopy (AES or XPS) traditionally applied for the analysis of surface chemical composition also allows us to draw a conclusion on surface morphology. Unfortunately, for silver chlorination, the situation appears to be rather complicated, and a few widely different models of surface morphology were suggested, based on AES and XPS data in Refs. [8,10–15].

It was established [10–14] that the formation of AgCl could be started only after completion of a chemisorbed chlorine monolayer. The maximum rate of AgCl growth was observed at 220–250 K [10–14]. The low-temperature growth of silver chloride on silver low-index crystalline planes was studied by AES, XPS, and thermal desorption spectroscopy (TDS) in Refs. [8,10–14]. The chloride phase growth observed on the silver surface in the temperature range 150–250 K has been interpreted as 2D [8,14] or 3D [12,13] AgCl crystallite formation. More sharp difference exists for interpretation of results for room- and higher-temperature behaviour of a chlorinated silver surface. Bowker et al. [10–13] concluded that at $250 < T < 500$ K, there was a dissolution of chlorine from the AgCl phase into the bulk of silver substrate which destroyed the AgCl film formed at low temperatures. As a result of the AgCl phase destruction, only a chlorine monolayer is left on the surface. Chlorine adsorption at these temperatures ($250 < T < 500$ K) also causes direct dissolution of chlorine into the bulk of silver, with only a monolayer remaining on the surface [10–13]. Wu et al. [15] interpreted their room-temperature results as the formation of 3D AgCl islands surrounded by an area of metallic silver patches and proposed chlorine dissolution into the bulk through this defect Ag layer. Andryushechkin et al. [8,14] concluded that the heating of 2D AgCl film formed at low temperature gives rise to its transformation into 3D AgCl islands surrounded by chemisorbed chlorine monolayer. No chlorine dissolution under the surface was supposed. Chlorine adsorption [14] or AgCl deposition [8] at room temperature also led to the formation of 3D AgCl islands surrounded by a chemisorbed chlorine layer.

In this study, we have used scanning tunnelling microscopy (STM) in combination with AES, LEED and TDS to compare the spectroscopic data with local topography of surface. The formation of chloride islands at room-temperature chlorination has been confirmed by direct STM observations. The identification of islands as the AgCl phase was made with AES and TDS measurements. It was also established that primary electrons in AES cause a tremendous transformation in silver chloride film morphology. A strong influence of middle-energy electrons on the silver chloride film could explain the discrepancies in interpretating previous electron spectroscopy data.

## 2. Experimental

All experiments were carried out in a UHV set-up consisting of analytical and STM chambers. The analytical chamber was equipped with cylindrical mirror analyser for AES (Riber OPC-200) and quadrupole mass-spectrometer (Riber Q-156) for TDS measurements. The STM chamber was equipped with a home-made room-temperature STM [16] and 3-grid optics for LEED. The samples and the STM tips could be easily moved from the analytical chamber to STM or LEED by means of a transfer system. The base pressure in both chambers did not exceed $2 \times 10^{-10}$ Torr.

The Ag(111) sample preparation procedure included repeated cycles of heating (20 min,

[1] NATO Linkage Program, grant #HTECH.LG951227.

800 K) and $Ar^+$ bombardment (1000 eV) up to the disappearance of C and S contamination in the Auger spectra. The temperature was measured by means of a chromel/alumel thermocouple mounted near the mass-spectrometer ionizer. In the course of the temperature measurements, the thermocouple was brought into contact with the face of the sample. The as-prepared surface showed a sharp LEED pattern ($1\times1$) and easily observed atomic terraces and steps in STM (Fig. 1). Molecular chlorine was introduced onto the sample face in the analytical chamber through the piezoelectric fine leak valve controlled by a computer. The chlorine beam enhancement factor was about 200.

The Cl $L_{2,3}VV$ (160–195 eV) and Ag $M_{4,5}VV$ (335–365 eV) Auger lines were acquired in the first derivative mode with a modulation voltage of 0.9 $V_{pp}$. The energy of the primary electron beam was 3 keV. The density of the target current (15 μA $cm^{-2}$) was chosen to avoid any damage to the surface during Auger spectra collection. TDS measurements were made for $Cl^+$, $Cl_2^+$, $Ag^+$, $AgCl^+$, $AgCl_2^+$, $Ag_2Cl^+$, $Ag_2Cl_2^+$, $Ag_3Cl_3^{++}$ ions with a linear heating rate of 2 K $s^{-1}$. Tungsten tips sharpened in situ by $Ar^+$ bombardment [17] were used for STM measurements.

## 3. Data treatment

To estimate the concentration of different surface compounds, three different analytic tools AES, TDS and STM were used in the experiments. If TDS or STM measurements provide information on this subject without any complex mathematical treatment (the integral of the TDS peak corresponds to the amount of desorbed molecules, and the STM image shows the size of the surface features), Auger measurements could give such information only after special treatment of the spectra. To identify chemical states on a surface during chlorination, we employ factor analysis treatment of Auger spectra (AES-FA) [18,19]. Here, we present a short description of this method of data treatment.

Factor analysis is a well-known statistical method that has been applied successfully in ana-

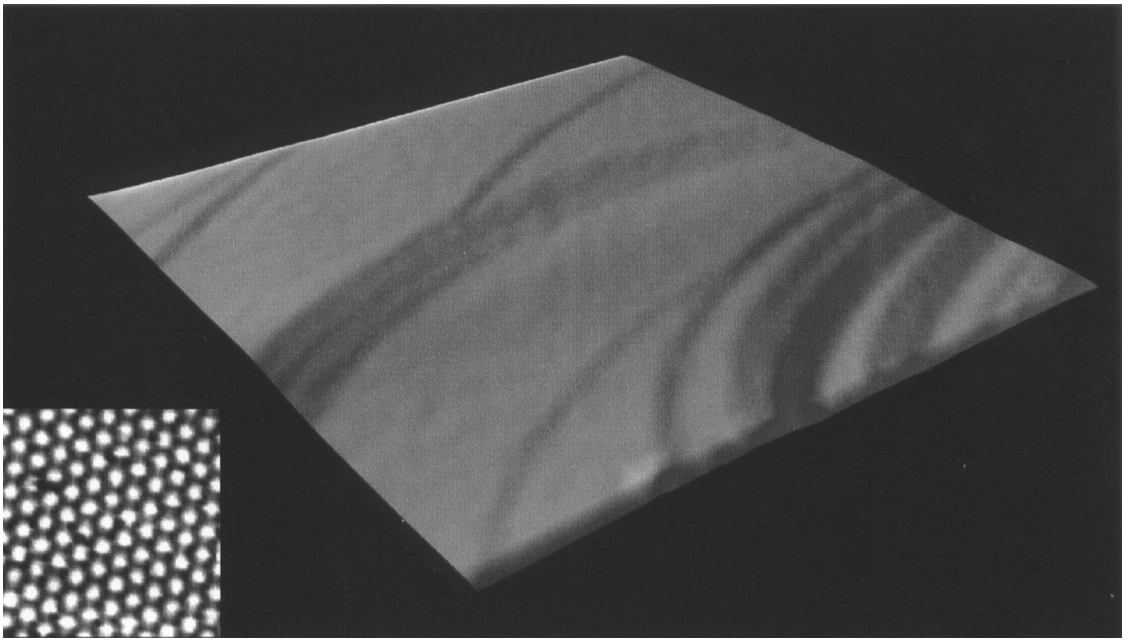

Fig. 1. STM image ($7100\times7100$ Å$^2$) of a clean Ag(111) surface. Insert: atomic resolution image of Ag(111)-($1\times1$) structure, $26\times28$ Å$^2$ ($U_t=50$ mV, $I_t=1$ nA). The interatomic distance is $3.0\pm0.15$ Å.

lytical chemistry [20]. Application of the factor analysis appeared to be useful when the total spectrum of the investigated system could be considered as a linear combination of the spectra of its components, with their concentrations being varied in the course of a process. It is important that the spectrum of the particular component be unique and independent of the component concentration in the system. Factor analysis allows both the number of independent components in the system to be determined and the behaviour of each component to be determined separately. AES is considered to satisfy the requirements mentioned above. A distinctive feature of the application of factor analysis to AES is a careful consideration of depth of emission of Auger electrons [8,14,18,19,21,22].

Factor analysis was introduced in AES by the pioneering work of Gaarenstroom [18,19] for depth profiling in thin films. To our knowledge, there are only a few papers in which factor analysis in Auger spectra has been applied to study the adsorption system, in particular O/Ni [21,22].

A detailed formalism of factor analysis can be found in Ref. [20]. In the first stage of factor analysis, the so-called principal component analysis (PCA), the number of relevant factors (components) is obtained. The measured Auger spectra are written to the data matrix ([$D$]) as rows. Each of the rows of [$D$] ($m$, $n$) consists of the signal intensities for the $m$ points on the energy scale for the array of $n$ spectra. The aim of the factor analysis is to break down the data matrix into a product of two matrices [$R$] and [$C$]:

$$[D]=[R]\cdot[C], \tag{1}$$

where the matrix [$R$] ($m$, $c$) contains Auger spectra of $c$ pure components in the system, and the matrix [$C$] ($c$, $n$) contains the concentrations of each of $c$ components in the array of $n$ spectra.

According to Ref. [20], the number of independent components in the system $c$ is equal to the number of the non-zero eigenvalues of a covariant matrix $[Z]=[D]^{T}[D]$. The indicator function (IND) [20] and the standard error in the eigenvalues (SE) [23] are used to determine the number of the eigenvalues statistically different from zero.

In the PCA stage, the pair of matrices ([$R^{\sim}$] and [$C^{\sim}$]) could be obtained, satisfying condition (1). As a rule, the pair of matrices [$R^{\sim}$] and [$C^{\sim}$] is an abstract solution of Eq. (1) without any direct physical meaning. However, using the target transformation procedure, it is possible to obtain the required matrices [$R$] and [$C$]. Formally, target transformation is a procedure for finding an appropriate matrix [$T$] that will transform [$C^{\sim}$] into [$C$] and [$R^{\sim}$] into [$R$] [20]:

$$[C]=[T][C^{\sim}], \tag{2}$$

$$[R]=[R^{\sim}][T]^{-1}. \tag{3}$$

To find the transformation matrix [$T$], one should have information on the physical and chemical properties of the investigated system. The matrix [$T$] can be obtained principally by two different test procedures ('target testing'). The procedure used more often is based on knowledge of the components in the system and their standard spectra. Spectra of the pure components form a standard matrix [$R^{*}$], which also must satisfy Eq. (3). Mathematically, the least-square fitting of the matrix [$R^{*}$] by the product $[R^{\sim}][T]^{-1}$ has to be performed for the calculation of the matrix [$T$]. Then, using Eq. (2), the matrix [$C$], containing the concentration dependencies of the components, can be easily calculated. The second way to calculate [$T$] is based on the knowledge or assumption of concentration dependencies. In this case, they form the matrix [$C^{*}$], which should be fitted by the product $[T][C^{\sim}]$ according to Eq. (2). Finally, the calculation of the matrix [$R$] is straightforward from Eq. (3).

## 4. Results and discussion

### 4.1. Silver chloride formation

The clean surface of Ag(111) is characterized by STM images presented in Fig. 1. A frame $7100\times7100$ Å$^2$ in size shows vast terraces separated by atomic steps or their cascades. The atomic-resolution image ($26\times28$ Å$^2$) containing the small area of a terrace is shown in the insert of Fig. 1. The Ag–Ag interatomic distance of

$3.0 \pm 0.15$ Å, as measured from the STM images, is in agreement with the table value of 2.87 Å [24].

Fig. 2 shows an STM image of the Ag(111) surface treated by molecular chlorine at a dose of 20 000 L ($1\ \mathrm{L} = 10^{-6}$ Torr s). The character of relief has been drastically changed after chlorine action. Beside the atomic terraces, the separated islands and colonies of them can be seen clearly. Wide ditches surround the islands. The untreated plateaux ($\sim 100$ Å in height) between the islands can be seen also (see the left part of Fig. 2a). We observed that the walls of the plateaux (ditches) have rectangular, square or hexagonal symmetry. They are different planes from the basic Ag(111). The large values of interatomic distances (larger than the Ag–Ag distances) and symmetry mean that some of them are (100), (110) planes covered by chlorine. We were unable to identify these atomic structures, but we believe that the observed structures are complex surface lattices formed by chemisorbed chlorine on corresponding planes. In Fig. 2b, a facet on the top edge of the wall is shown. A rectangular lattice can be clearly seen. We have also obtained atomic-resolution STM images for the top of the plateaux and bottom of the ditches (see Fig. 2c). They both exhibit the Ag(111)-$(17 \times 17)$-Cl structure observed earlier at a saturated monolayer coverage of chlorine on Ag(111) [25]. LEED patterns corresponding to the Ag(111)-$(17 \times 17)$-Cl structure [25] were also

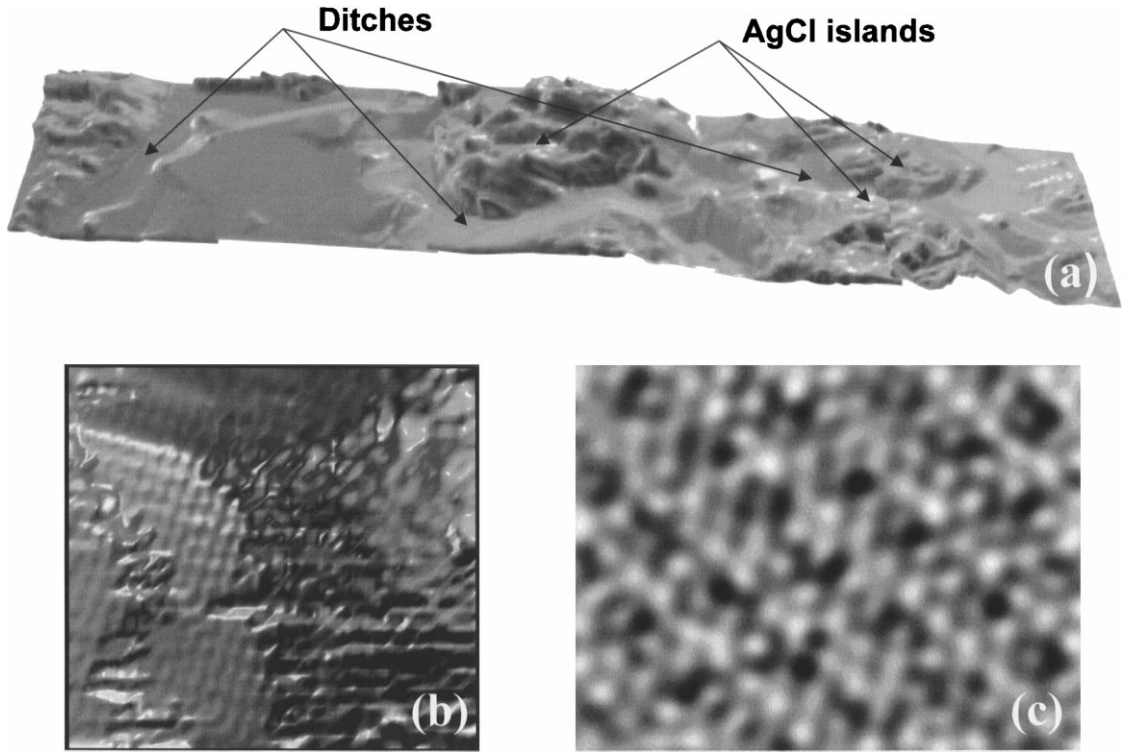


Fig. 2. STM images of Ag(111) surface after 20 000-L dose of $Cl_2$. (a) Panoramic image, $20\,000 \times 8000$ Å$^2$; (b) $196 \times 183$ Å$^2$ image of ditch/wall area, showing a facet (top of pyramid) with three planes. Left and upper ones have rectangular lattice of size approximately $7 \times 10$ Å. We propose them to be $<110>$ planes covered by chemisorbed chlorine. We believe this modulation of electron density to reflect the interaction between chlorine and substrate lattices (analogous to Ag(111)- $(17 \times 17)$-Cl [24]) and correspond to double diffraction LEED pattern [11]. Two terraces separated by monoatomic step are clearly seen on the left plane. The boundary between the planes looks perfect and lies along atomic rows. The right plane (without atomic resolution) was found to be (111) with $(17 \times 17)$-Cl structure. The transition region between (110) and (111) planes contents many atomic defects. (c) Atomic resolution image of Ag(111)-$(17 \times 17)$-Cl structure (observed both on the top of plateau and on the bottom of ditch), $51 \times 44$ Å$^2$ ($U_t = -1.3$ V, $I_t = 0.1$ nA). Additional periodicity of $\sim 10$ Å [25] is clearly seen.

observed on the surface after chlorine action at a dose of up to 100 000 L, and that is why we identify the coverage between the islands as a saturated monolayer of chemisorbed chlorine.

To assign the islands to a AgCl chemical compound, we had to compare spectral data obtained by AES and TDS with the STM data of a chlorinated surface. Analysis of the STM images allowed us to determine both the sizes of the separated islands (height and base area) and the surface area occupied by islands. Of course, this estimation is not very precise (about 10–15% of accuracy), but we were able to determine a general change in island sizes versus the chlorine dose. For each chlorine dose, the treatment was made for 5–8 $\mu m^2$ of a surface. We could not exactly estimate the influence of the shape of STM tip on the shape and size of islands, but we believe that the distortions caused by STM tips are not noticeable. The typical STM tip apex had a radius of 20–40 Å and an angle of 20–25° [17].

To determine the surface area occupied by the AgCl phase from Auger spectra, we applied the AES-FA approach, successfully used earlier for silver chlorination [14] and AgCl deposition on Ag(111) [8]. Fig. 3 shows the spectra of Cl $L_{2,3}VV$ and Ag $M_{4,5}VV$ lines for a continuous AgCl film, Ag(111) covered by a chemisorbed chlorine ($Cl_{ads}$) monolayer and for chlorinated Ag(111) surface presented in Fig. 2. The large chemical shifts for AgCl lines in comparison with line positions for chemisorbed chlorine and silver substrate were a strong argument for factor analysis application [8,14]. A detailed description of the AES-FA procedure for the case of silver chlorination can be found in Ref. [14]. As a result of FA treatment (the main steps are described in Section 3), we were able to separate the AgCl phase from chemisorbed chlorine and metallic silver and to draw its concentration as a chlorine dose function [14]. At the submonolayer stage of chlorine adsorption ($\theta \leq 1$), we found only the chemisorbed chlorine. At $\theta > 1$, AgCl was formed on the surface (the AgCl component appeared and reached the saturation level) simultaneously with the disappearance of $Cl_{ads}$. We have established in Refs. [8,14] that the AgCl phase is formed on the surface instead of $Cl_{ads}$, and a process of silver

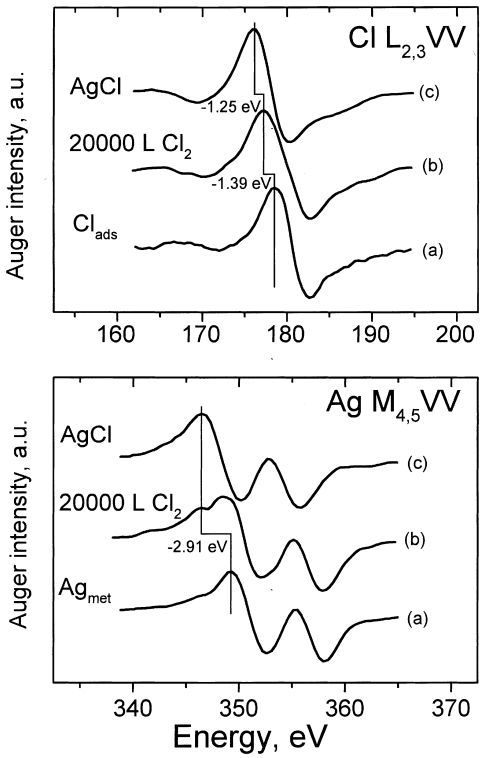


Fig. 3. Cl $L_{2,3}VV$ and Ag $M_{4,5}VV$ AES lines of chlorinated Ag(111) surface: (a) covered by a chlorine monolayer; (b) AgCl island film, 20 000 L dose of chlorine at room temperature; (c) AgCl continuous film.

chloride formation occurs as Clads⇔CuCl transition. Since $Cl_{ads}$ intensity is directly proportional to the area occupied by chemisorbed chlorine (one layer thickness), the surface area covered by AgCl islands is determined as a comparative change in intensity of the $Cl_{ads}$ component for a saturated monolayer coverage ($\theta = 1$) and for the surface partially covered by the chloride islands ($\theta > 1$).

To measure the relative amount of silver chloride on the surface by TDS, we used the intensity of the $Ag_2Cl^+$ fragment in the AgCl sublimation peak [8,10,14]. TD spectra of the chlorinated Ag(111) are presented in Fig. 4. It was determined in Ref. [10] that the spectra can contain two peaks: a broad peak with a maximum at 750 K, corresponding to chlorine monolayer desorption, and a sharp peak at 670 K, corresponding to AgCl film sublimation. The monolayer chlorine desorption peak can be described as being a result of sublima-

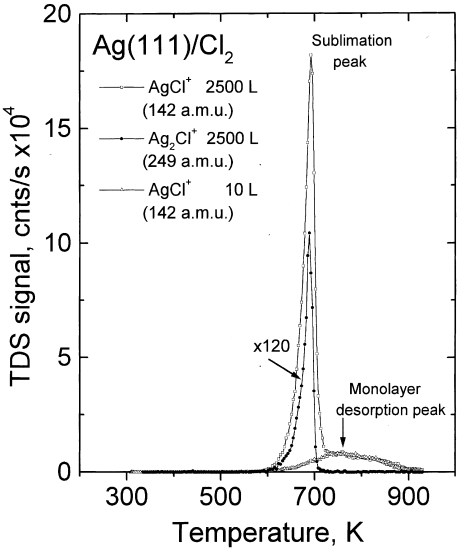


Fig. 4. Thermal desorption spectra of a chlorinated Ag(111) surface. △: $AgCl^+$ ion, chlorine monolayer coverage, 10 L; □: $AgCl^+$ ion, AgCl island film, 2500 L; ●: $Ag_2Cl^+$ ion, AgCl island film, 2500 L.

tion of the upper silver layer bound with chlorine. This peak consists of AgCl molecules only (see Table 1). The bonds of the first silver layer with the second layer in the substrate lattice are reduced due to the strong silver–chlorine interaction. That is why the sublimation process of chlorinated silver (upper silver layer) is started at a lower temperature (~550 K) than that for clean silver (~860 K).

It can be clearly seen from Table 1 that the AgCl film sublimation peak has additional heavier fragments like $Ag_2Cl^+$, $Ag_2Cl_2^+$, and $Ag_3Cl_3^{++}$ in comparison with the monolayer desorption peak. Monomer, dimer, and trimer chloride molecules were found in Ref. [26] to be the major sublimation products of AgCl substrate. We believe that the AgCl sublimation peak from the chlorinated Ag(111) surface also consists of monomer, dimer, and trimer chloride molecules. In this connection, it should be noted that the chlorine desorption peak integral for $AgCl^+$ ions cannot be directly used as a reference for calibration of surface chloride coverage because of the different distribution of the ion intensities for monomer, dimer or trimer molecules [12]. In Ref. [10], the authors found only monomer chloride for both TDS peaks and additional silver ions in the sublimation peak, and used $AgCl^+$ fragment intensity for surface chloride calibration. From our point of view, these TDS data could be used only for a relative estimation of the amount of surface chloride.

Fig. 5 shows the dependence of AgCl coverage (the surface area covered by islands), measured by

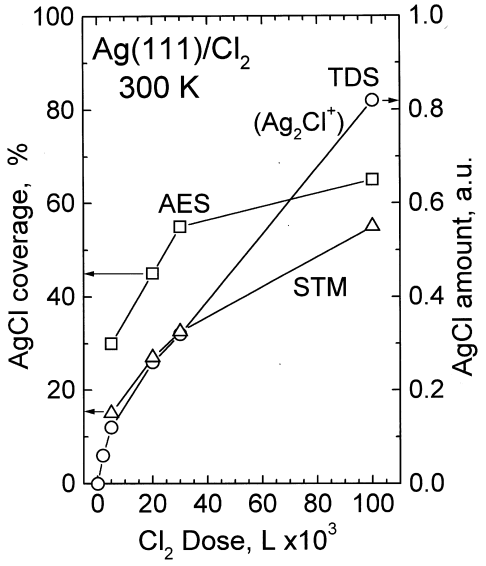


Fig. 5. $Cl_2$ dose dependence of AgCl coverage measured by STM (△), AES (□) and AgCl amount measured by TDS (○).

Table 1
Relative intensities of ion fragments obtained in thermal desorption spectra of Ag(111) chlorinated surface

| Dose | AgCl sublimation peak | | | | | | Monolayer desorption peak | |
|---|---|---|---|---|---|---|---|---|
| | $Ag^+$ 107 amu | $AgCl^+$ 142 amu | $Ag_2^+$ 214 amu | $Ag_2Cl^+$ 249 amu | $Ag_2Cl_2^+$ 284 amu | $Ag_3Cl_3^{++}$ 213 amu | Ag 107 amu | $AgCl^+$ 142 amu |
| 2500 L | 75.3 | 100 | 4.2 | 0.83 | 0.01 | 0.12 | 20 | 100 |

STM and AES, and the dependence of relative amount of surface chloride obtained from TDS versus $Cl_2$ dose. The general trend of all curves is clear: the intensities increase with chlorine dose.

The STM data in Fig. 2 provide direct evidence of the existence of islands appearing as a result of chlorine action. The highly correlated behaviour of the AES, TDS and STM curves in Fig. 5 proves that the islands are the silver chloride compound.

The results presented allow us to select the correct morphology model of AgCl growth among those predicted in earlier papers. In Refs. [8,14,15], the authors explained the electron spectroscopy results by the formation of AgCl islands. In this sense, it corresponds to the present STM results. The chlorine dissolution into the bulk of silver and absence of AgCl phase on the surface suggested by Bowker et al. [10,13] do not correspond to the results from Figs. 2 and 5. Of course, we cannot exclude the probability of chlorine dissolution, but none of the STM data confirms this. In Ref. [15], the authors also predicted the partial dissolution of chlorine into the bulk through the destroyed surface around the AgCl islands. By STM, we observed only an atomic smooth surface around AgCl islands (Fig. 2). Moreover, atomic structure on the bottom of ditches around the AgCl islands corresponds to the structure of a perfect saturated chlorine monolayer [25] and does not differ from the surface areas far from the islands. Thus, we can conclude that STM results fully confirm a morphology model of chlorinated silver surface presented in Refs. [8,14]: at room temperature, AgCl islands coexist with the chemisorbed chlorine monolayer.

From the analysis of several STM frames recorded for a 3000–5000 L chlorine dose, we concluded that the nucleation of islands usually occurs on surface defects such as atomic steps and their crossing. Preferably, the islands occupy places along the atomic step, but this does not mean that a AgCl phase cannot be formed on a flat surface. We found that at a lower-temperature chlorination (240 K), small (30–60 Å) 2D AgCl islands were formed on flat atomic terraces far from the steps (see Ref. [27]). At room-temperature chlorination, we have not found such islands on a flat surface. Moreover, the surface with a small density of defects could be kept without chloride at large doses (see the smooth plateau on the left-hand side of Fig. 2). The growth of islands at room temperature is accompanied by the formation of ditches around the islands. We suppose that the ditches are caused by chloride diffusion from a periphery of the reaction zone to the centre to form the island. At room temperature, the islands grow in a 3D shape due to surface tension. We observed the formation of ditch walls of low-index planes (Fig. 2b) different from the basic (111) one. The possible explanation of such an effect could be found in a strong decrease in reaction rate after removal of surface defects and creation of perfect planes.

The interesting feature observed by Bowker et al. [10,11,13] was the large $Ag^+$(107 amu)/$AgCl^+$(142 amu) ratio in the sublimation peak ($\sim$0.3) in comparison with the monolayer peak ($\sim$0.05) in TDS. In the present paper, a similar difference is also observed for sublimation and monolayer peaks in TDS: 0.75 and 0.20, respectively (Table 1). In Ref. [10], the specific silver chloride structure formed upon Ag(111) chlorination was suggested and supported in Ref. [11] for Ag(110)/$Cl_2$. In Refs. [12,13], based on XPS measurements, another model, such as Stranski–Krastanov growth of silver chloride on Ag(110) and Ag(100), was supposed. Nevertheless, the question on presence of extra silver atoms in silver chloride structure requires an answer. On the one hand, the data presented in Table 1 show that chloride is sublimated as mono-, di- and trimers. We tried to estimate the contribution of di- and trimer molecules in ion fragmentation of the sublimation peak, but it appeared to be rather small [26]. On the other hand, our recent atomic resolution STM images obtained for 2D AgCl islands grown on Ag(111) at 240 K [27] showed the presence of small Ag clusters on the top of AgCl islands. Such silver clusters could desorb simultaneously with AgCl islands and disturb the observed mass spectrum of AgCl sublimation peak because the Ag ions from silver atoms or clusters could overlap and effectively enhance the relative intensity of silver ion fragments ($Ag^+$ and $Ag_2^+$) in silver chloride species.

### 4.2. Electron beam action

It is of interest to know the origin of the discrepancy in the interpretation of electron spectroscopy data by different groups [8,10–15]. Taking into account silver chloride to be a very photosensitive material [28] we proposed that the primary electrons of energy 1–3 keV (AES) or X-ray irradiation (XPS) could disturb the silver chloride formed on the surface. To study an influence of medium energy electrons on chlorinated silver surface a special model experiment was carried out. Really, in STM images we have observed a very strong electron beam action on AgCl islands morphology.

Fig. 6 shows the $20\,800 \times 7800$ Å$^{-2}$ images of the 100 000 L chlorinated Ag(111) surface before (Fig. 6a) and after (Fig. 6b) 3-keV electron beam irradiation at a dose of 0.1 C cm$^{-2}$ (100 s × 1 mA cm$^{-2}$). The change in surface topography appears to be considerable: instead of silver chloride island film consisting of several islands with a height of 600–1200 Å, two giant (2500 and 2800 Å in height) chloride islands are observed after electron action. In Fig. 6a, dark parts correspond to the untreated silver surface covered by the chlorine monolayer; the grey–white colour scale indicates the chloride phase. In Fig. 6b, two types of objects could be separated: giant islands and large terraces at 400 and 150 Å levels in comparison with the dark parts. STM indicated that the terraces were covered by a chlorine monolayer with Ag(111)-$(17 \times 17)$-Cl structure. As a result, the average chloride coverage (estimated for an area of 15 μm$^2$) decreased from 55–60% (Fig. 5) to 6–9%. It was also found that the electron beam action could be easily recognized with the naked eye: at the place of beam scanning, the silver glance has been restored, whereas the rest of the surface has been kept matt.

The degradation of the chlorinated surface detected by a decrease in Cl ($L_{2,3}VV$)/Ag

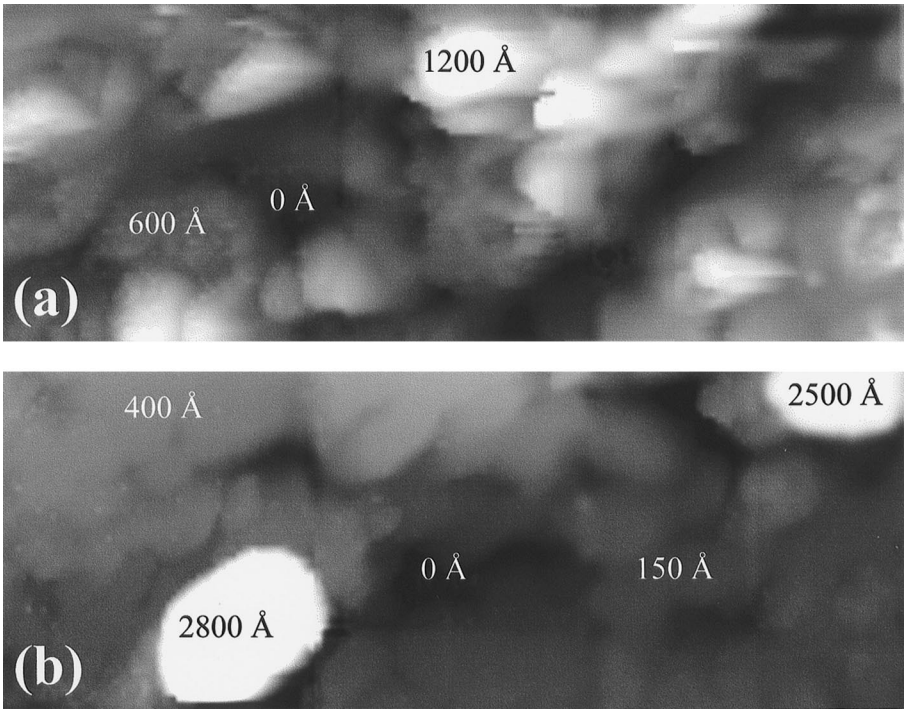


Fig. 6. STM image of Ag(111) surface chlorinated with a 100 000-L dose of $Cl_2$. $20800 \times 7800$ nm$^2$ (a) before electron action and (b) after electron action of 0.1 C cm$^{-2}$ dose ($U_t = -1.5$ V, $I_t = 0.2$ nA). (Different parts of the surface are shown.) The heights of the features are indicated.

($M_{4,5}VV$) Auger ratio under the action of electron irradiation is shown in Fig. 7 for different primary electron densities. An electron beam with a density of $10^{-4}$–$10^{-3}$ A cm$^{-2}$ causes a decrease in the Cl/Ag Auger ratio from 1.6 to 0.72, corresponding to a change in chloride coverage from 65% (Fig. 5) to 5–10%, as estimated with AES-FA. It follows from Fig. 7 that the electron beam with a current density of 5 mA cm$^{-2}$ gives rise to a total surface degradation in 1 min or less. Therefore, the application of AES appears to be ineffective for the chloride phase determination on the silver surface. Moreover, for these regimes of measurements, the destructive character of AES is obvious.

The typical electron density values usually used in AES are 1–100 mA cm$^{-2}$. We suppose that the electron density of several mA cm$^{-2}$ could correspond to the electron beam current of 0.5 μA employed in Refs. [10,11]. As shown above, this current density leads immediately to damage of the initially formed chloride layer, and therefore, correct AES detection of the chloride phase was impossible. AES results in Refs. [8,14] were also obtained for a surface modified by primary electrons (10 mA cm$^{-2}$ density). Only the use of a factor analysis treatment for AES data allowed us [8,14] to separate AgCl and chemisorbed chlorine in the case of such strong electron action. It was found that the relative surface chloride coverage at room temperature does not exceed 10% [14]. This small amount of AgCl could not be detected by AES without FA application. We also suppose that the action of X-ray radiation on a surface during XPS measurements [12,13,15] is strong enough to disturb the silver chloride film.

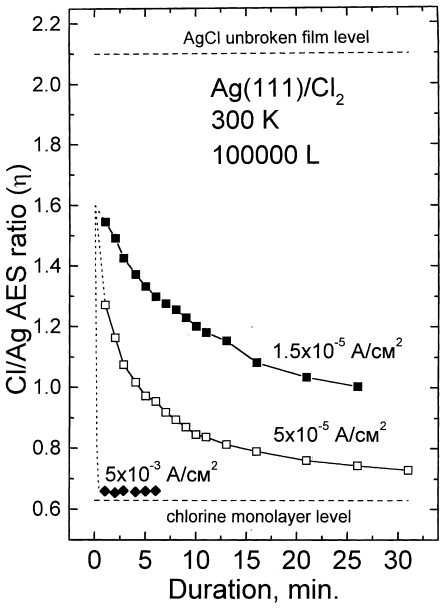


Fig. 7. Time dependence of the Cl $L_{2,3}VV$/Ag $M_{4,5}VV$ intensity ratio under a primary electron action of 3-keV energy obtained for different electron beam densities. The lines in the range inaccessible for measurements are drawn by dotted curves. The signal level for monolayer coverage and that for the continuous chloride film are shown by dashed horizontal lines.

In this study, we have taken into account the electron damage. AES results presented in Fig. 5 were collected with a primary electron density of 15 μA cm$^{-2}$. Only one spectrum for each chlorine dose was recorded. The duration of one spectrum collection was less than 2 min, and distortion did not exceed a few percent (the first point in the corresponding curve in Fig. 7). After every Auger spectrum recording, we changed the place on the sample surface.

It is necessary to discuss the experimental arguments presented in Refs. [10–13] in more detail in support of the model of chlorine dissolution in the bulk of silver at temperatures of 300–600 K and following chlorine segregation at 600–650 K. A Cl/Ag ratio diminishing in the 300–600 K range and the appearance of a sharp peak of Cl/Ag ratio at 600–650 K were experimentally indicated in thermal programmed (TP) AES [10,11] and XPS [13] data of a low-temperature formed AgCl film.

Similar TP AES curves (Cl/Ag ratio) obtained with different primary electron densities for AgCl film (20 000 L of chlorine) are presented in Fig. 8. Note that the Cl/Ag ratio ($\eta$) correctly reflects the AgCl coverage between continuous AgCl film ($\eta = 2.1$) as 100% and chlorine monolayer ($\eta = 0.62$) as 0% (see Fig. 7). The initial AgCl coverage was about 40%. Curve 1 corresponds to heating under the action of a very-low-intensity electron beam (0.25 μA cm$^{-2}$). No features similar those presented in Refs. [10–13] were observed. The curve starts from $\eta = 1.4$ and falls slowly to $\eta = 1.0$ in the 300–670 K range. At $T > 670$ K, the signal disappears due to AgCl sublimation and chlorine desorption processes (see Fig. 4). Before the curve

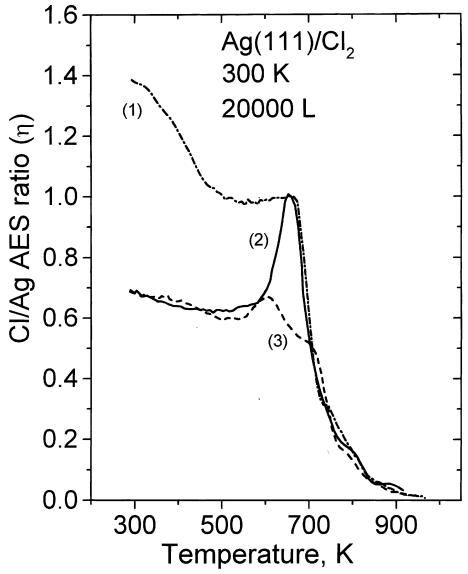


Fig. 8. Temperature dependence of Auger lines Cl $L_{2,3}VV$/Ag $M_{4,5}VV$ intensity ratio with a linear heating rate of 3.7 K $s^{-1}$ obtained for different primary current densities of 3-keV electrons. 1: measurement with $\rho = 0.25$ μA $cm^{-2}$; 2: preliminary action at 300 K with $\rho = 12.4$ mA $cm^{-2}$ during 2 min, measurement with $\rho = 0.25$ μA $cm^{-2}$; 3: measurement with $\rho = 12.4$ mA $cm^{-2}$.

2 collection, the surface was subjected to a high-density electron beam action (12.4 mA $cm^{-2}$) for a few minutes at 300 K. In accordance with data in Fig. 7, the AES signal obtained after such a strong electron action becomes close to the monolayer value in several seconds. Then, to exclude electron action during heating, curve 2 was recorded with a low-density current (0.25 μA $cm^{-2}$). Curve 2 starts from $\eta = 0.66$ and demonstrates a sharp peak at 640 K, with its intensity being equal to that of curve 1 at the same temperature. Curve 2 looks similar to the curves from Refs. [10–13]. On the contrary, curve 3 was recorded under a high-density electron beam action (12.4 mA $cm^{-2}$) during heating. There was no preliminary electron action. Curve 3 also has a peak at $T \sim 600$ K but with a low intensity of $\eta = 0.7$

On the basis of the results presented in Fig. 8, we suggest the following interpretation. The temperature action causes the agglomeration of AgCl islands with saturation of island sizes at $T \sim 500$–650 K. This process looks like a continuation of temperature transformation of a 2D silver chloride film (grown at low temperature) at room-temperature annealing [8,10–14]. The driving force of such agglomeration could be a surface diffusion of AgCl molecules to achieve a surface energy minimum. This process is reflected in curve 1. Curve 2 could reflect another process. At room temperature, preliminary electron beam action (12.4 mA $cm^{-2}$) leads to the formation of 'giant' islands (see Fig. 6b). We do not know the mechanism of such action, but we suppose that these 'giant' islands do not correspond to thermodynamical equilibrium of chlorinated silver surface. The STM and AES data evidently show that the islands formed by electron beam action at room temperature are much larger than the islands formed at $T \sim 600$ K without electron action. The behaviour of curve 2 can be unambiguously interpreted as a transition from 'giant' AgCl islands at room temperature to smaller islands at 600 K with a higher coverage of AgCl. We also do not know the mechanism of the transition. Perhaps the surface melting of silver chloride could be responsible for such a transformation at $T \sim 570$–650 K. To follow this transition, we selected the electron densities of the lowest (curve 2) and the highest (curve 3) values achieved in our experiment. The low-intensity peak observed in curve 3 reflects the simultaneous action of both the temperature and the electrons. We also found that the intermediate electron density beams gave intensities of the peak at $T \approx 640$ K between the values for curve 2 and curve 3. We believe that the TP AES and XPS curves (signal decrease at 300–600 K, peak at $\sim 650$ K) from Refs. [10–13] can be explained by the simultaneous action of temperature and electrons (or X-ray radiation), and their behaviour reflects the AgCl islands transformations on the surface but not the chlorine dissolution into the bulk and following surface segregation.

The model of silver chloride formation proposed in Refs. [8,14] and confirmed by STM data in the present paper can also explain the results of special experiment performed in Ref. [11]. In this experiment, an ion bombardment of chloride film formed upon 110 K chlorination of Ag(110) and annealed at 300 K was carried out both at 110 K

and at 300 K. The first case showed a rapid removal of chlorine (90 s) down to a Cl/Ag ratio of ~0.4, and the latter a slow removal (30 min) to approximately the same Cl/Ag level. The TP AES [11] showed the difference. After low-temperature bombardment, the peak at 600–650 K remained on the curve, whereas after room-temperature bombardment, it disappeared. The segregation of chlorine from the bulk at room temperature and its simultaneous removal by bombardment were used in Ref. [11] as an explanation for the absence of a peak. Such segregation was forbidden thermodynamically in low-temperature ion bombardment, and the main amount of chlorine was kept in the bulk contributing to the TP AES peak with further heating. In the framework of the AgCl islands model [8,14], this behaviour is explained in terms of surface diffusion of chlorine atoms from chloride islands instead of bulk diffusion and segregation.

To understand the mechanism of electron action, additional experiments and theoretical studies are needed. However, one more feature of this phenomenon also needs to be described. The area of the surface opened after chloride island removal under the action of electrons looks like a system of large terraces separated by short channels (Fig. 6b). As mentioned above, the orientation of the terraces was found to be (111) with the structure Ag(111)-(17 × 17)-Cl. The different symmetry of chlorine monolayer for the walls of the channels observed by STM could be assigned to (100), (110), or (111) silver planes covered by a chlorine monolayer. Taking into account that room temperature is too low for diffusion of silver atoms, we think that these STM images reflect the correct topography of interface AgCl/Ag(111). The channels can correspond to 'roots' of chloride islands formed in the course of chlorination. In addition to our own interest in the mechanism of electron action, it could be useful to study the topography of AgCl/Ag interface at different stages of the chlorination process.

## 5. Conclusions

In this paper, we have presented direct evidence of AgCl island formation on the Ag(111) surface upon molecular chlorine adsorption at room temperature. The findings are as follows:

- In the STM images of Ag(111) treated by large doses of molecular chlorine, we observed both islands surrounded by ditches and untreated plateau.
- The correlation of AES data (relative surface are occupied by silver chloride), TDS data (total amount of AgCl) on the one hand and STM measurements (direct observation of islands growth) on the other hand proves that the islands are the silver chloride compound.
- The surface area between the AgCl islands is covered by a chemisorbed chlorine monolayer with structure (17 × 17)-Cl on the Ag(111) plane and a complex (unidentified) structure on the ditch walls, which demonstrate square or rectangular symmetry.

It has been established that primary electrons in AES induce transformation of silver chloride film morphology:

- Using an electron beam action with a dose density of less than 0.1 C $cm^{-2}$, we observed tremendous changes in the AgCl island film: instead of islands, with a height of 600–1200-Å, occupying approximately 60% of the surface (chloride coverage $\theta_{AgCl} \approx 0.6$), giant islands, with a height of 2500–3000 Å ($\theta_{AgCl} < 0.1$), have been formed.
- The time changes of Auger lines intensity for chlorinated Ag(111) obtained for different primary electron densities ($10^{-5}$–$10^{-2}$ A $cm^{-2}$ range) strongly correspond to a decrease in AgCl coverage.

We believe that strong influence of medium-energy electrons on silver chloride film is an origin of different interpretation of electron spectroscopy data in Refs. [8,10–15]. We have shown that the temperature-programmed behaviour of the Auger Cl $L_{2,3}VV$ curve observed in Refs. [10,11] can be easily explained in terms of AgCl island size changes on the silver surface due to the combined action of primary electrons and high temperature. At an extremely low electron density ~1 μA $cm^{-2}$, the temperature-programmed Auger curves reflect the usual coalescence process of chloride islands only.

## Acknowledgements

This work was supported in part by the Russian Foundation of Basic Research (grant #18233), Ministry of Science and Technologies (grants #96-3.15, and #316), Ministry of Education (grant # K-0513) and NATO (Linkage grant #HTECH.LG951227).

## References

[1] R.B. Grant, R.M. Lambert, J. Catal. 92 (1985) 364.
[2] R.B. Grant, C.A.J. Harbach, R.M. Lambert, S. Aun Tan, J. Chem. Soc., Faraday Trans. I 83 (1987) 2035.
[3] C.T. Campbell, J. Catal. 99 (1986) 28.
[4] G. Rovida, F. Pratesi, M. Maglietta, E. Ferroni, Jpn. J. Appl. Phys. 2 (Suppl. 2) (1974) 117.
[5] P.J. Goddard, R.M. Lambert, Surf. Sci. 67 (1977) 180.
[6] Y.Y. Tu, J.M. Blakely, J.Vac. Sci. Technol 15 (1978) 563.
[7] C.T. Campbell, 1998, private communication.
[8] B.V. Andryushechkin, K.N. Eltsov, V.V. Martynov, Poverkhnost (1999) in press (in Russian).
[9] R.G. Jones, Progr. Surf. Sci. 27 (1988) 25.
[10] M. Bowker, K.C. Waugh, Surf. Sci. 134 (1983) 639.
[11] M. Bowker, K.C. Waugh, Surf. Sci. 155 (1985) 1.
[12] M. Bowker, K.C. Waugh, B. Wolfindale, G. Lamble, D.A. King, Surf. Sci. 179 (1987) 254.
[13] M. Bowker, J. Electron Spectrosc. Relat. Phenom. 37 (1986) 319.
[14] B.V. Andryushechkin, K.N. Eltsov, V.V. Martynov, Phys. Low Dim. Struct. 6 (1995) 1.
[15] K. Wu, D. Wang, J. Deng et al., Surf. Sci. 264 (1992) 249.
[16] K.N. Eltsov, A.N. Klimov, S.L. Priadkin, V.M. Shevlyuga, V.Yu. Yurov, Phys. Low Dim. Struct. 7/8 (1996) 115.
[17] K.N. Eltsov, V.M. Shevlyuga, V.Yu. Yurov, A.V. Kvit, M.S Kogan, Phys. Low Dim. Struct. 9/10 (1996) 7.
[18] S.W. Gaarenstroom, Appl. Surf. Sci. 7 (1981)
[19] S.W. Gaarenstroom, Appl. Surf. Sci. 26 (1986) 561.
[20] E.R. Malinowski, D.G. Howery, Factor Analysis in Chemistry, Wiley, New York, 1980.
[21] S. Hofmann, J. Steffen, Surf. Sci. 202 (1988) L607.
[22] S. Hofmann, J. Steffen, Surf. Int. Anal. 14 (1989) 59.
[23] Z.Z. Hugus, A.A. El-Awady, J. Phys. Chem. 75 (1971) 2954.
[24] J. Donohue, The Structure of the Elements, Wiley, New York, 1974.
[25] B.V. Andryushechkin, K.N. Eltsov, V.M. Shevlyuga, V.Yu. Yurov, Surf. Sci. 407 (1998) L633.
[26] L.C. Wagner, R.T. Grimley, J. Phys. Chem. 70 (1972) 2819.
[27] B.V. Andryushechkin, K.N. Eltsov, V.M. Shevlyuga, Surf. Sci., in press.
[28] T.H. James, The Theory of Photographic Process, Macmillan, New York, 1977.